Ion acceleration in underdense plasmas by ultra-short laser pulses

Ion acceleration in underdense plasmas by ultra-short laser pulses

A Lifschitz[1], **F Sylla**[1,2], **S Kahaly**[1,5], **A Flacco**[1], **M Veltcheva**[1],
G Sanchez-Arriaga[3], **E Lefebvre**[4] **and V Malka**[1]

[1] Laboratoire d'Optique Appliquée, ENSTA, CNRS, Ecole Polytechnique, UMR 7639, F-91761 Palaiseau, France
[2] SourceLAB SAS, 86 rue de Paris, F-91400 Orsay, France
[3] Escuela Técnica Superior de Ingenieros Aeronáuticos, Universidad Politécnica de Madrid, E-28040 Madrid, Spain
[4] CEA, DAM, DIF, F-91297 Arpajon, France
E-mail: agustin.lifschitz@ensta-paristech.fr

Abstract

We report on the ion acceleration mechanisms that occur during the interaction of an intense and ultrashort laser pulse ($I\lambda^2 > 10^{18}$ W cm^{-2} μm^2) with an underdense helium plasma produced from an ionized gas jet target. In this unexplored regime, where the laser pulse duration is comparable to the inverse of the electron plasma frequency ω_{pe}, reproducible non-thermal ion bunches have been measured in the radial direction. The two He ion charge states present energy distributions with cutoff energies between 150 and 200 keV, and a striking energy gap around 50 keV appearing consistently for all the shots in a given density range. Fully electromagnetic particle-in-cell simulations explain the experimental behaviors. The acceleration results from a combination of target normal sheath acceleration and Coulomb explosion of a filament formed around the laser pulse propagation axis.

Keywords: laser plasma interaction, ion acceleration, plasma modeling

[5] Present address: Service des Photons, Atomes et Molcules, CEA, DSM/IRAMIS, CEN Saclay, F-91191 Gif sur Yvette, France

Several studies [1–5] carried out over the past decade have demonstrated the potential of ultra-intense $(I\lambda^2 > 10^{18}\,\mathrm{W\,cm^{-2}\,\mu m^2})$ lasers as compact ion accelerators from laser–plasma relativistic interaction. The interest in such a field stems not only from potential applications (fast ignition [6], ion therapy [7]) thanks to the characteristics of the accelerated bunches (low-emittance [8], quasi-monoenergetic spectra [9, 10]), but also from fundamental investigations of the interaction and plasma properties through electron and ion spectral analysis [11–16].

Most of these works were performed by focusing the laser beam over a thin solid target, which allows us to get very sharp density ramps and high accelerating fields [2–5, 10]. An alternative is to use gaseous targets, which enable work at a high repetition rate, to control the accelerated species and the plasma profile in a simple manner. This is the promising approach adopted in recent studies using very energetic infrared CO_2 lasers [17, 18], for which suitable gas targets can be fabricated. However, the production of gas jets with overcritical density for near-infrared laser systems and sharp edges constitutes a technological challenge that has just started to be taken up [19], a fact that has limited the development of the gas target approach up to now.

Reported acceleration experiments using gas targets and near-infrared laser systems were performed in the underdense regime ($n_e < n_c$, with n_e and n_c, respectively, the electron and critical plasma densities), and with laser pulse durations much larger than the inverse electron plasma frequency [1, 20–22]. In this regime, the fastest ions gain their radial momenta from Coulomb explosions, when the laser field is still present and bores a channel by expelling plasma electrons. The accelerated ions continue to drift undisturbed due to their inertia when the quasineutrality is restored as the electrons come back to screen the electrostatic field after the pulse is gone. In the first experiments, a 50 J–0.9 ps laser pulse focused over a gas jet with $n_e = 5 \times 10^{19}\,\mathrm{cm^{-3}}$ allowed the production of a few MeV ions with exit angles around 100° to the axis of propagation and Maxwellian distribution [1]. The contrast between the obtained Maxwellian spectrum and the one expected from a Coulomb explosion (flat with a peak at the energy cutoff) was attributed to the superposition of Coulomb explosion-like spectra for the different values of laser intensity occurring along the pulse propagation in the gas jet [1, 20]. Experiments performed with larger laser energies (180 J) and higher densities ($n_e > 10^{20}\,\mathrm{cm^{-3}}$) lead to ion energies of the order of 10 MeV, with plateau-like spectra [21]).

Longitudinal acceleration was achieved by raising the laser energy (340 J) [22–25]. In this case, a radial component with a cutoff of 10 MeV, arguably coming from the Coulomb explosion of the ion channel, coexisted with a beam accelerated longitudinally with a cutoff of 40 MeV. The longitudinal acceleration is caused by a target normal sheath acceleration (TNSA)-like mechanism, possibly enhanced by the azimuthal magnetic field existing at the plasma boundary [23–25].

In this paper, radial acceleration from underdense He plasma ($n_e \sim 10^{19}\,\mathrm{cm^{-3}}$) with short pulses is demonstrated for the first time. Observations with single-shot diagnostics of spectral patterns close to quasi-monoenergetic helium ion bunches (cutoff $E_0 \sim 200$ keV) are presented and discussed. Owing to the ultrashort laser pulse duration, comparable to the inverse electron plasma frequency, the direct laser-induced Coulomb explosion of a uniform positively-charged core from laser channeling is likely to be an incomplete picture for depicting the momentum transfer on the ion response timescale. The ions gain their radial momenta essentially after the pulse passage [26]. The short pulse excites a strongly nonlinear wakefield, which will radially

accelerate ions and produce an annular radial ion density profile (see equation (8) in [27]). At high densities and high laser intensities, electrostatic effects result in the compression of ions situated close to the axis forming a filament, which later Coulomb explodes [28]. For a longer time, when the fast inner ions outrun the slow outer ions, a collisionless shock can form in the phase space, with significant modification of the final energy distribution [28, 29].

In the experiment, an ultrashort (duration $\tau = 35$ fs) linearly polarized pulse from the Laboratoire d'Optique Appliquée Ti:sapphire Salle Jaune laser [30] carrying $E_L = 800$ mJ was focused with an $f/10$ of the f-axis parabolic mirror to a $20\,\mu$m $(1/e^2)$ focal spot, giving a laser intensity of $I_0 = 1.3 \times 10^{19}$ W cm^{-2}. The supersonic He jet density was varied from 0.8 to 5.6×10^{19} cm^{-3} (0.5% to 3.5% of n_c) and had a $700\,\mu$m diameter. The ratio between the laser power P_L and the critical power P_c for relativistic self-focusing ($P_c = 16.2 \; n_c/n_e$ GW) was between 7 and 50 (the plasma and Rayleigh length values were comparable).

The interaction was spatially adjusted above the nozzle by means of plasma emission imaging (10 μm spatial resolution). The top-view and side-view images allow the positioning of the beam, respectively, along a diameter of the jet and at a chosen height from the nozzle (see figure 1). Ion emission measurements were carried out at 0° and ~80° from the laser propagation axis through a $100\,\mu$m diameter pinhole (solid acceptance 1.2×10^{-8}sr) with a Thomson parabola spectrometer coupled to 40 mm imaging microchannel plate chevron assembly (two microchannel plates (MCPs) and a phosphor screen). This very narrow angle of collection efficiently filters out ions accelerated at different directions from the normal laser axis. A linearized thermo-electric-cooled 16-bit CCD camera (1024 × 1024 px) enables single-shot recordings of scintillating traces and thus shot-to-shot statistical analysis of the ion spectra. The electric gains of the MCP assembly were set to preserve the full dynamics of 16-bit pictures from saturation and keep the signal-to-noise ratio better than 50:1. With a 2:1 magnification, the system gives a $500\,\mu$m pinhole image of the jet on the first MCP plane (10 pixels on the CCD image), which allows us to regard the source as point-like and the ion emission as laminar. The detection threshold is ~48 keV for He^{2+} and ~10 keV for He$^+$.

No ion was detected in the forward direction (see figure 1), i.e. no He^{2+} ion with energy above the detection threshold (48 keV) leaves the jet at 0°. Both ionic species, on the other hand, were detected with the spectrometer at 80°. A raw picture from a single laser shot is presented in figure 2 and shows striking gaps in the spectral traces and the presence of both species He$^+$ and He^{2+}. However, the ratio $I_0/I_{sb}\left(\text{He}^{2+}\right) > 100$, ensures full ionization of gas in the focal volume (with $I_{sb}\left(\text{He}^{2+}\right)$ the threshold intensity for suppression of the potential barrier). Calculations with $I_0/I_{sb}\left(\text{He}^{2+}\right) = 100$, using sequential field ionization of neutral gas by a Gaussian laser pulse, show fully ionized plasma over a radius of ~200 μm. Within the energy range 20–200 keV, elastic collisions of He^{2+} projectiles with He atoms are largely dominated by a one-electron capture process with a typical capture cross-section $\sigma_c \sim 10^{-16}$ cm^2 [31]. Thus, He$^+$ ions are very likely to stem from single electron capture of radially streaming He^{2+} in the outer layers of the jet (hence the importance of the gas profile in detecting both species). Moreover, we found that the ratio between the number of He$^+$ and He^{2+} ions grows with the gas density, in agreement with the electron capture hypothesis.
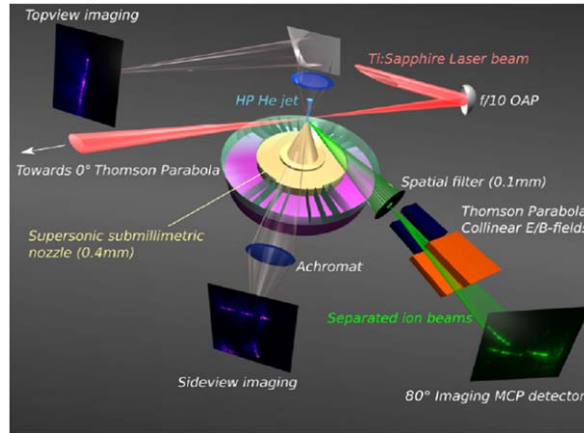
Figure 1. The experimental setup with characteristic plasma emission images (top view and side view with a stretched pulse of 300 fs) and ion emission spectral recordings (with a compressed pulse of 30 fs).
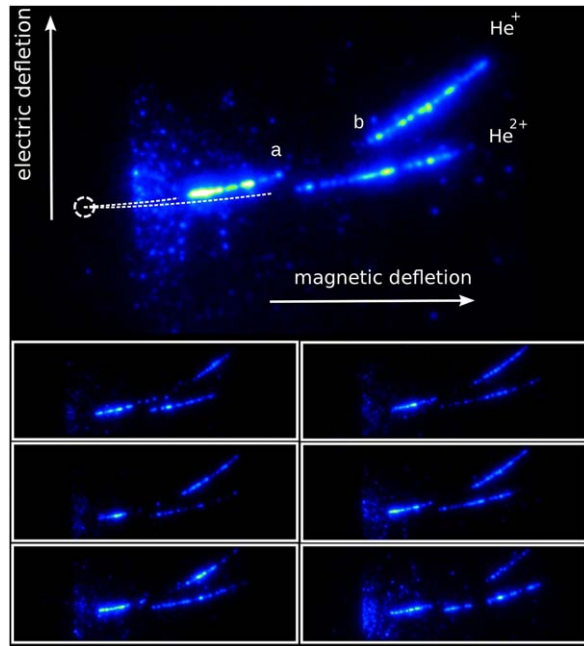
Figure 2. Raw pictures from the Thomson parabola at 80°, with each one corresponding to a single shot for $n_e = 2.8 \times 10^{19}$ cm^{-3} with $I = 1.3 \times 10^{19}$ W cm^{-2}. The neutral blob (dashed circle) is filtered out and the dotted lines indicate the fit dispersion traces for each species. The dispersive magnetic field reads B = 0.25 T. Points a and b are located at 55 and 28 keV in the He$^+$ spectrum.

The He$^+$ spectrum presents an upper branch above point a and a lower branch below point b ($\Delta E_{ab} \sim 27$ keV, see figure 2). In this gap region, the signal falls below the noise level (see figure 3(a) and the inset). An energy gap is also observed between the least energetic detected alpha $\sim$60 keV and the lower limit of detection in the He^{2+} spectrum $\sim$48 keV. Both upper branches (above the gaps) lie precisely within the range 60–200 keV, supporting the electron

(a) Experiment

(b) Simulation
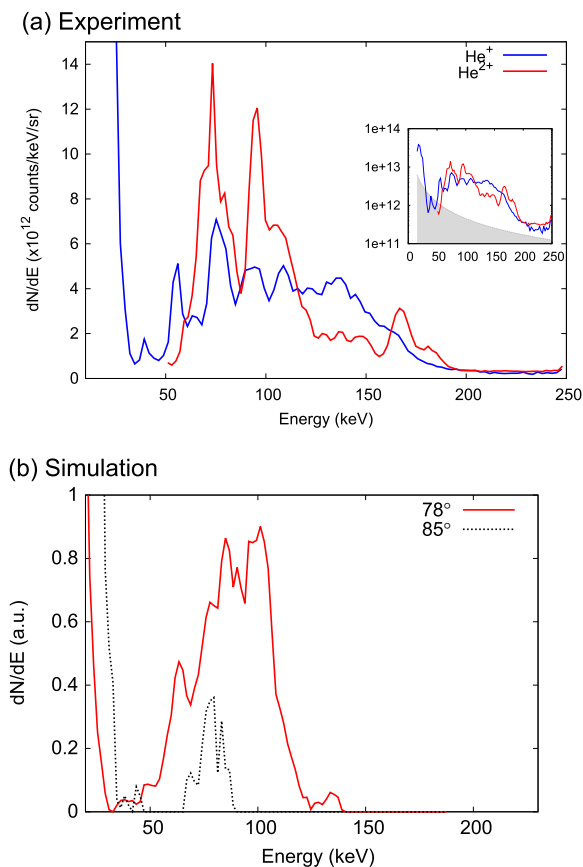
Figure 3. (a) Experimental spectra extracted from the top raw image in figure 2 (relative counting, bin width *dE* = 2 keV). Inset (logscale): cutoff ∼200 keV, signal-to-noise ratio 50 : 1 (shaded below the dark noise level). (b) The energy spectrum of He^{2+} ions emitted at 85° and 78° from the simulation.

capture hypothesis. The main features of the spectrum, a gap and a cutoff around 200 keV, are similar for densities ranging from 0.8 to 3 × 10^{19} cm^{-3} (0.5% to 2% of n_c). Moreover, changing the laser polarization direction does not affect the spectra. The number of ions reaching the MCP is relatively low (roughly of the order of a few hundreds) because of the very small angular acceptance of the detector.

To gain an insight into the mechanism of ion acceleration, we carry out a numerical study of the interaction process via particle-in-cell (PIC) simulations, performed using the fully electromagnetic PIC code Calder-Circ [32]. In this code, Maxwell equations are solved by projecting over a basis of Fourier modes. Few modes are enough to accurately describe the laser evolution and the wakefield, resulting in simulations needing much less computational resources than fully 3D simulations. The modelling of the acceleration process requires the inclusion in the simulation box of the whole gas jet, and the continuation of the simulations far beyond the wakefield decay time, precluding the use of too many numerically expensive Cartesian 3D simulations. The simulations performed here include two Fourier modes.

The parameters of the simulations correspond to those used in the experiments: a laser wavelength $\lambda_0 = 0.8 \, \mu$m with a duration of 30 fs full width at half maximum. The laser spot

waist is $20\,\mu$m, and the laser intensity is $I = 1.2 \times 10^{19}\,\mathrm{W\,cm^{-2}}$ (normalized vector potential $a_0 = 2.4$). The laser pulse is linearly polarized in the y direction. The cell size in the longitudinal direction is $\Delta z = 0.628\,k_0^{-1}$ and in the radial direction $\Delta r = 1.5\,k_0^{-1}$. The plasma is fully ionized (composed of He^{2+} and electrons), with the hyper-Gaussian density longitudinal profile given by $n_e = 0.015\,n_c \exp\left(-\left((r\,(\mu\mathrm{m}) - 440)/363\right)^6\right)$. The simulation box is composed of $13\,000\,(\mathrm{longitudinal}) \times 600\,(\mathrm{radial})$ cells.

The obtained spectrum for radially accelerated ions (figure 3(b)) nicely reproduces the main features of the experimental spectrum (figure 3(a)). The spectra present low and high energy branches. The first one has a Maxwellian-like distribution with a cutoff around 40 keV. The high energy branch presents a broad peak, which goes from 50 to 150 keV for an exit angle of 78°. These values are close to the low and high energy cutoffs of the upper branch in the experiment. Simulation also shows that ions leaving the jet at 0° have energies lower than 30 keV. This value lies below the detection threshold for He^{2+} (48 keV), but above the one for He^+ (10 keV). However, their conversion to He^+, which would allow their detection by the Thomson parabola at 0°, is precluded because these ions do not transverse a region of neutral or partially ionized gas. The simulated spectrum does not visibly change by changing the laser polarization direction, in agreement with the experimental result.

The two energy branches found in the spectrum correspond to two distinct ion populations accelerated by different mechanisms and in different regions of the gas jet. The low energy branch is composed of ions accelerated in the central region of the gas jet by the radial field existing in the wakefield. The high energy branch, on the other hand, corresponds to ions accelerated in the plasma sheath that is created in the falling density ramp of the plasma. As the longitudinal plasma density gradient is not sharp enough, the radial field is larger than the longitudinal one, and the main acceleration is radial. Ions are pushed towards the axis by the quasi-electrostatic field in the sheath, and Coulomb explosion of the formed filament further accelerates the ions.

The acceleration of the low energy ion population results from the fact that the average radial field in a non-linear wakefield does not vanish. Close to the axis (typically for $r < 1\,\mu$m) the time averaged radial field is negative, especially in the presence of electrons injected and accelerated in the wakefield [28]. The Thomson parabola at 0° was not able to detect these electrons because its magnetic field is too large. However, a test made using a double magnet scheme shows the presence of relativistic electrons longitudinally accelerated in the wakefield, although the setup was not well suited to recovering the electron spectrum.

Beyond the central region, the average field over the ions in the pulse trail is positive. The result of the central focusing field and that surrounded by a region of the defocusing field is the formation of a channel of low density with a central filament. The channel radially expands roughly ballistically up to the formation of a sharp edge on the outer shell of the channel, which cannot be screened, and the emergence of an electrostatic shock [28, 29], which will redistribute the energy between ions. Simulations made with a very narrow gas jet and meshes with higher radial resolution show that to accurately describe the effect of the shock on the spectrum requires the use of smaller radial sizes. However, these simulations show that the shock has little effect on the cutoff energy itself, which will remain around 30 keV. The filament, on the
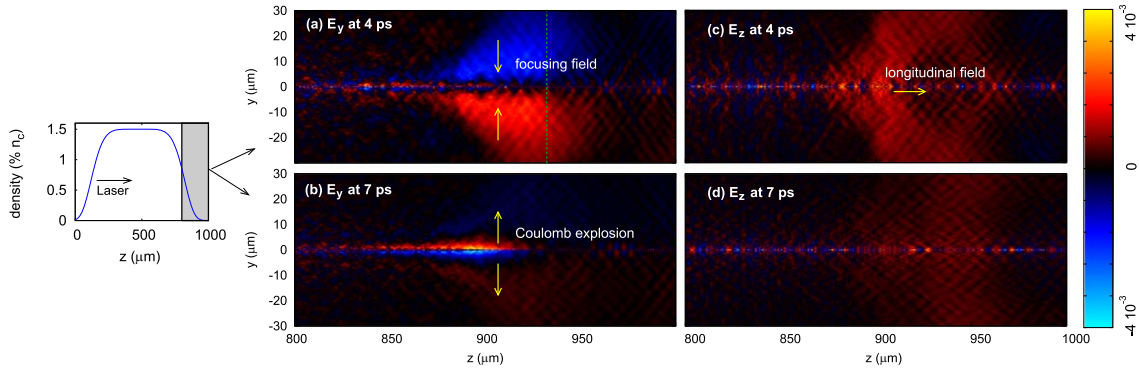
Figure 4. The transverse (left) and longitudinal (right) electric field (in units of a_0) in the falling density ramp of the plasma at 4 ps (top) and 7 ps (bottom). The plotted region is indicated in gray in the inset, and shows the density profile of the gas jet. The dashed line roughly indicates the position of the interface plasma/vacuum.
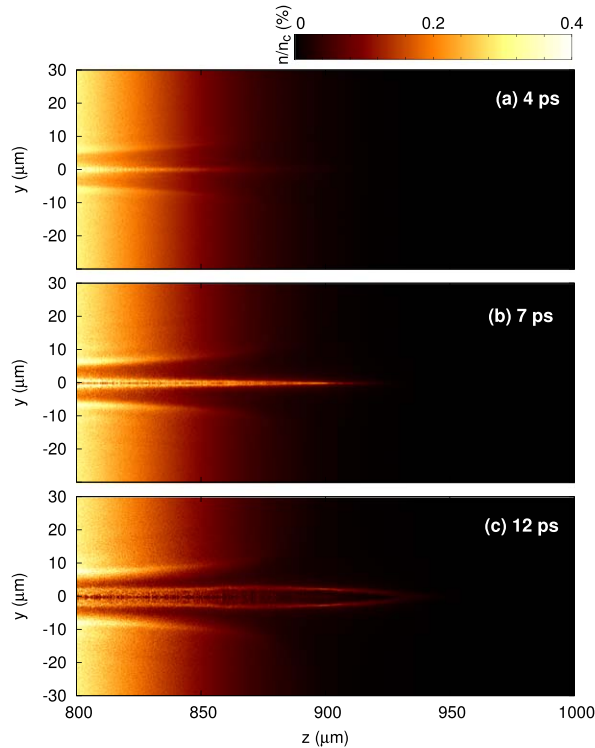
Figure 5. Zoomed images of the ion spatial density distribution around the falling density ramp and in the midplane $x = 0$ at three different times.

other hand, will pinch ballistically up to a sub-micrometric radius, and then Coulomb explode. The cutoff energy after the explosion is close to 40 keV.

The high energy branch of the spectrum corresponds to ions accelerated in the falling density ramp of the gas jet, where a TNSA-like sheath is formed. The dilute electron population is not able to screen the ion charge, and a radially focusing and longitudinally accelerating (for positive ions) electric field will arise (figures 4(a) and (c)) and stand for a few ps. The presence

of a stable magnetic structure, visible in the simulation, could also contribute to the sustainability of the sheath by limiting the electron transport [23–25]. The radial field focuses ions coming from $r < 10\,\mu$m towards the axis, forming a filament (figure 5(b)). When the filament reaches its minimum radius, its peak density becomes 20 times larger than the unperturbed original density, whereas for the filament formed in the plasma core, the maximum density is only two times larger than the unperturbed one. The weak screening will result in a stronger Coulomb explosion (figures 5(c) and 4(b)). The result of this explosion is a sudden radial acceleration with an energy cutoff of ~150 keV. Due to the longitudinal field (figure 5(b)), ions will leave the target with an angle smaller than 90°. The longitudinal acceleration also results in a finite minimal energy for ions collected at a given angle, and therefore the gap between the spectra of the two ion populations. Ions above 50 keV are emitted with angles between ~55° and ~85°, symmetrically distributed around the laser propagation axis. The solid angle of the resulting emission is around π sr. Because of this very broad emission, the characterization of the accelerated ion population in terms of beam properties (emittance, length, etc) is not very meaningful.

For densities higher than 2% n_c and up to the highest density explored (3.5% n_c), the gap disappears and the spectrum becomes Maxwellian-like, a trend also found in simulations. The reason for this is the rise in the energy cutoff of ions accelerated in the plasma core, which becomes higher than 50 keV, thus filling the gap. The spectrum of the two ion populations are therefore overlapped. These results will be detailed in future work.

In conclusion, novel aspects of laser ion acceleration have been revealed in a regime where the laser pulse duration is close to ω_p^{-1}. An ion population radially accelerated in the falling density ramp of the gas jet was identified. The energy gap between this population and a less energetic one accelerated in the wakefield is a signature of the presence of a longitudinal field in the falling density ramp. This study also suggests that to get more energetic ions in the forward direction, one has to enhance the longitudinal electric field, for example by using targets with much steeper density gradients.

Acknowledgments

References

[1] Krushelnick K *et al* 1999 Multi-MeV ion production from high-intensity laser interactions with underdense plasma *Phys. Rev. Lett.* **83** 737–40
[2] Clark E L, Krushelnick K, Zepf M, Beg F N, Tatarakis M, Machacek A, Santala M I K, Watts I, Norreys P A and Dangor A E 2000 Energetic heavy-ion and proton generation from ultraintense laser-plasma interactions with solids *Phys. Rev. Lett.* **85** 1654–7
[3] McKenna P *et al* 2004 Characterization of proton and heavier ion acceleration in ultrahigh-intensity laser interactions with heated target foils *Phys. Rev.* E **70** 036405
[4] Fuchs J *et al* 2007 Laser-foil acceleration of high-energy protons in small-scale plasma gradients *Phys. Rev. Lett.* **99** 015002

 [5] Henig A *et al* 2009 Radiation-pressure acceleration of ion beams driven by circularly polarized laser pulses *Phys. Rev. Lett.* **103** 245003

 [6] Roth M *et al* 2001 Fast ignition by intense laser-accelerated proton beams *Phys. Rev. Lett.* **86** 436–9

 [7] Bulanov S V and Khoroshkov V S 2002 Feasibility of using laser ion accelerators in proton therapy *Plasma Phys. Rep.* **28** 453–6

 [8] Cowan T E *et al* 2004 Ultralow emittance, multi-MeV proton beams from a laser virtual-cathode plasma accelerator *Phys. Rev. Lett.* **92** 204801

 [9] Ter-Avetisyan S, Schnürer M, Nickles P V, Kalashnikov M, Risse E, Sokollik T, Sandner W, Andreev A and Tikhonchuk V 2006 Quasimonoenergetic deuteron bursts produced by ultraintense laser pulses *Phys. Rev. Lett.* **96** 145006

[10] Hegelich B M, Albright B J, Cobble J, Flippo K, Letzring S, Paffett M, Ruhl H, Schreiber J, Schulze R K and Fernandez J C 2006 Laser acceleration of quasi-monoenergetic MeV ion beams *Nature* **439** 441–4

[11] Wickens L M, Allen J E and Rumsby P T 1978 Ion emission from laser-produced plasmas with two electron temperatures *Phys. Rev. Lett.* **41** 243–6

[12] Ter-Avetisyan S, Schnürer M, Busch S, Risse E, Nickles P V and Sandner W 2004 Spectral dips in ion emission emerging from ultrashort laser-driven plasmas *Phys. Rev. Lett.* **93** 155006

[13] Allen M *et al* 2003 Proton spectra from ultraintense laser–plasma interaction with thin foils: experiments, theory, and simulation *Phys. Plasmas* **10** 3283–9

[14] Mora P and Grismayer T 2009 Rarefaction acceleration and kinetic effects in thin-foil expansion into a vacuum *Phys. Rev. Lett.* **102** 145001

[15] Daido H, Nishiuchi M and Pirozhkov A S 2012 Review of laser-driven ion sources and their applications *Rep. Prog. Phys.* **75** 056401

[16] Macchi A, Borghesi M and Passoni M 2013 Ion acceleration by superintense laser-plasma interaction *Rev. Mod. Phys.* **85** 751–93

[17] Palmer C A J *et al* 2011 Monoenergetic proton beams accelerated by a radiation pressure driven shock *Phys. Rev. Lett.* **106** 014801

[18] Haberberger D, Tochitsky S, Fiuza F, Gong C, Fonseca R A, Silva L O, Mori W and Joshi C 2011 Collisionless shocks in laser-produced plasma generate monoenergetic high-energy proton beams *Nat. Phys.* **8** 95

[19] Sylla F, Veltcheva M, Kahaly S, Flacco A and Malka V 2012 Development and characterization of very dense submillimetric gas jets for laser-plasma interaction *Rev. Sci. Instrum.* **83** 033507

[20] Sarkisov G S, Bychenkov V Yu, Novikov V N, Tikhonchuk V T, Maksimchuk A, Chen S-Y, Wagner R, Mourou G and Umstadter D 1999 Self-focusing, channel formation, and high-energy ion generation in interaction of an intense short laser pulse with a He jet *Phys. Rev.* E **59** 7042–54

[21] Wei M S *et al* 2004 Ion acceleration by collisionless shocks in high-intensity-laser–underdense-plasma interaction *Phys. Rev. Lett.* **93** 155003

[22] Willingale L *et al* 2006 Collimated multi-MeV ion beams from high-intensity laser interactions with underdense plasma *Phys. Rev. Lett.* **96** 245002

[23] Willingale L *et al* 2007 Willingale *et al* reply *Phys. Rev. Lett.* **98** 049504

[24] Willingale L *et al* 2008 Longitudinal ion acceleration from high-intensity laser interactions with underdense plasma *IEEE Trans. Plasma Sci.* **36** 1825–32

[25] Bulanov S V and Esirkepov T Zh 2007 Comment on 'Collimated multi-MeV ion beams from high-intensity laser interactions with underdense plasma' *Phys. Rev. Lett.* **98** 049503

[26] Andreev N E, Gorbunov L M, Kirsanov V I, Nakajima K and Ogata A 1997 Structure of the wake field in plasma channels *Phys. Plasmas* **4** 1145–53

[27] Gorbunov L M, Mora P and Solodov A A 2001 Plasma ions dynamics in the wake of a short laser pulse *Phys. Rev. Lett.* **86** 3332–5

[28] Popov K I, Rozmus W, Bychenkov N, Yu V, Naseri N, Capjack C E and Brantov A V 2010 Ion response to relativistic electron bunches in the blowout regime of laser-plasma accelerators *Phys. Rev. Lett.* **105** 195002

[29] Macchi A, Ceccherini F, Cornolti F, Kar S and Borghesi M 2009 Electric field dynamics and ion acceleration in the self-channeling of a superintense laser pulse *Plasma Phys. Control. Fusion* **51** 024005

[30] Flacco A *et al* 2010 Comparative study of laser ion acceleration with different contrast enhancement techniques *Nucl. Instrum. Methods* A **620** 18–22

[31] Shah M B and Gilbody H B 1985 Single and double ionisation of helium by H^+, He^{2+} and Li^{3+} ions *J. Phys.* B **18** 899

[32] Lifschitz A F, Davoine X, Lefebvre E, Faure J, Rechatin C and Malka V 2009 Particle-in-cell modelling of laser-plasma interaction using Fourier decomposition *J. Comput. Phys.* **228** 1803–14